



Long-fiber reinforced thermoplastic composite lattice structures: Fabrication and compressive properties



Bo Xu^a, Sha Yin^{b,c,*}, Yang Wang^a, Hongfu Li^a, Boming Zhang^a, Robert O. Ritchie^{d,e}

^a School of Materials Science & Engineering, Beihang University, Beijing 100191, China

^b School of Transportation Science & Engineering, Beihang University, Beijing 100191, China

^c Advanced Vehicle Research Center, Beihang University, Beijing 100191, China

^d International Research Centre for Advanced Structural & Biomaterials, Beihang University, Beijing 100191, China

^e Department of Materials Science & Engineering, University of California, Berkeley, CA 94720, USA

ARTICLE INFO

Article history:

Received 15 November 2016

Received in revised form 14 February 2017

Accepted 2 March 2017

Available online 4 March 2017

Keywords:

Lattice structure

Additive manufacturing

Thermoplastic composites

Mechanical properties

ABSTRACT

Recyclable lightweight materials with advanced processing techniques are essential for the sustainable development of future transportation. Thermoplastic composite lattice structures were developed to meet this demand. An additive manufacturing method is presented here to fabricate such lattice structures by reversible assembly of several long-fiber reinforced thermoplastic composite parts (LFTCPs) which were economically processed by injection molding. The resulting thermoplastic lattice structures (density of $30 \text{ kg}\cdot\text{m}^{-3}$) assembled with different sequences and connections are structurally evaluated and compared. Out-of-plane compression tests revealed that their mechanical properties were more sensitive to the presence of the connections rather than their assembly sequence, although their structural failure mode was always brake of inclined struts followed by fracture of the horizontal struts. Potential solutions to the problem of internal stresses, induced during assembly, are also explored by designing novel LFTCPs. The novel fabrication route for thermoplastic lattice structures will improve the prospects for their industrial application.

© 2017 Elsevier Ltd. All rights reserved.

1. Introduction

With the energy crisis and environmental pollution as major worldwide problems, stringent regulations in CO₂-emission and materials recyclability are becoming increasingly important in the automotive and transportation industries. In this regard, the application of lightweight materials is an effective route for sustainable development of automotive structures, particularly with the increasing use of composite materials. In contrast to other major applications of these materials, such as in aerospace engineering where the focus has been on properties and reliability, the future vehicle industry, such as for automotive, recoverable rockets, etc., tends to pay equal attention to manufacturing cost, time and uniformity, leading to their search for new lightweight materials with a high level of productivity and recycling potential.

Architected lattice materials are mechanical metamaterials with periodically patterned micro-structures and high strength-and stiffness-to-weight ratios. Such materials can be constructed

with topologies exhibiting properties greatly superior to those by their stochastic analogues (e.g., foams) [1–4]. Cellular geometries that provide the highest effective modulus and strength are stretch-dominated with no bending of the individual truss members. Also, the resulting effective modulus and strength of ideal stretch-dominated structures will scale linearly with relative density [5]. Over the past decade, such lattice materials have been presented as an exciting prospect for lightweight, multifunctional materials, and indeed they have found several applications, such as for airframes and sandwich panels for air blast protection, because of their superior specific strength, stiffness, large interconnected open space and potential for energy absorption [6–11]. In this regard, lattice composites which are fiber-reinforced composites combined with lattice topologies, have further attracted particular interest as they can enhance specific mechanical properties in engineered systems compared to their metallic counterparts [12–14]. Numerous manufacturing techniques have been developed for these lattice composite materials, such as hot press molding [13,15], weaving [16,17], expansion [18] and interlocking [14], although their complexity and requirements of custom tooling, pressurization for consolidation and prolonged heating for matrix curing have made these manufacturing processes both expensive

* Corresponding author at: School of Transportation Science & Engineering, Beihang University, Beijing 100191, China.

E-mail address: shayin@buaa.edu.cn (S. Yin).

and time-consuming. In 2013, a reversible assembly, additive manufacturing, method was introduced by Cheung et al. [19] to fabricate cuboctahedron (body-centered cubic, BCC, type) lattice by using many small identical parts as regular building blocks. Specifically, the thermoset composite digital elements that these authors designed were made by filament winding; the resulting cellular composite materials were reported to possess an extremely large measured modulus for an ultralight material [19].

Compared to their thermoset counterparts, thermo-plastic composites have an advantage in recyclability which is crucial for advanced vehicle industry [20]. Long-fiber reinforced thermoplastics (LFT) are usually prepared by an injection process using LFT pellets which are individual granulates with length of 10–25 mm sliced from continuous fibers with a polymer matrix surrounding them by pultrusion process. Furthermore, the development of long-fiber reinforced thermoplastics have undergone significant progress of late with consistently high surface quality and high impact resistance; accordingly, these additional economic benefits have markedly promoted their application [21–23]. In this study, we present a means to manufacture architected thermoplastic composites for high volume and low cost applications by using an additive manufacturing assembly methodology based on the methodology of Cheung et al. [19]. Distinct from the thermoset digital elements used in Ref. [19], we used long-fiber reinforced thermoplastic composite parts (LFTCPs), which were obtained by injection molding; these provided improved surface quality and a considerable cost saving compared to winding. We examine here the compressive behavior of such thermoplastic composites lattice structures with emphasis on the effects of assembly sequence and joint connection.

2. Methods

2.1. Lattice fabrication

A design of digital elements (LFTCPs), similar to that reported by Cheung et al. [19], was first used (Fig. 1a), with each element having four circular sections (tabs), four struts and a locally central hole for connection requirement. As noted above, the LFTCPs were manufactured using an LFT injection molding process, with carbon-fiber reinforced polypropylene (PP-LCF30) LFT granulates, prepared by co-mingling and melt-impregnation techniques to give an initial fiber length of ~10 mm and fiber volume content of ~30%. LFT using carbon fibre reinforcement, not only offer more reduction in weight, higher strength and effective modulus values,

but also enhances fatigue and creep properties and provides high electrical and thermal conductivities than glass fiber counterparts. LFTCPs and connection pins were manufactured using a mold and injection molding machine with a screw diameter larger than 40 mm to ensure the desired fiber length. During processing, the melt temperature was around 240 °C, and the mold temperature remained constant at 100 °C.

Subsequently, the thermoplastic composite lattice truss materials were assembled with mass-produced LFTCPs with mechanical fastening connections, according to the build-up method depicted in Fig. 2d. During the assembly process, four tabs from four different elements were constrained to meet at the central hole of the fifth element which was perpendicular to the other four. Two LFT pins (shown in Fig. 2c) or nylon cable ties were embedded orthogonally through the four tabs to serve as connections.

The specific sequence was determined from the joint. The relative location of the tabs in the local center hole is defined as 1–2–3–4 from up to down (left figure of Fig. 2e), and then the placement of the corresponding struts in the coordinate system is termed as the assembly order (a typical sequence is 1–4–2–3, as shown in the right figure of Fig. 2e).

2.2. Relative density

A schematic drawing of the representative unit cell of a specific assembly sequence without mechanical fastening is shown in Fig. 1b. Fig. 1a defines all the relevant geometric parameters of the BCC lattice structure. Assuming that the added weight of the mechanical connections can be ignored, the relative density $\bar{\rho}$ is given by the ratio of the solid volume to that of the unit cell:

$$\bar{\rho} = \frac{V_s}{V^*} = \frac{3t_1(4t_2^2 + 16t_1t_2 - t_1^2 + 4t_1l_1 + \pi D_1^2 - \pi D_2^2)}{L^3}, \quad (1)$$

where D_1 and D_2 are the respective outer and inner diameters of round section, l_1 is the strut length, l_2 is the side length of the locally central hole, l_3 is the distance between the center of the central hole and that of the round section, t_1 is the thickness of the struts, t_2 is the width of the central hole, and L represents the side length of the cubic occupied by the unit cell (Fig. 1b). Only an open-cell lattice with low density ($\bar{\rho} < 0.1$) is considered in this study [24]. For the assembly shown here, the side length of the local center hole is equal to the outer diameter of the round section and is four times thickness of the struts, which gives $l_2 = D_1 = 4t_1$. To simplify the assembly process, relatively large sizes, $t_1 = 5$ mm, $t_2 = 5.5$ mm

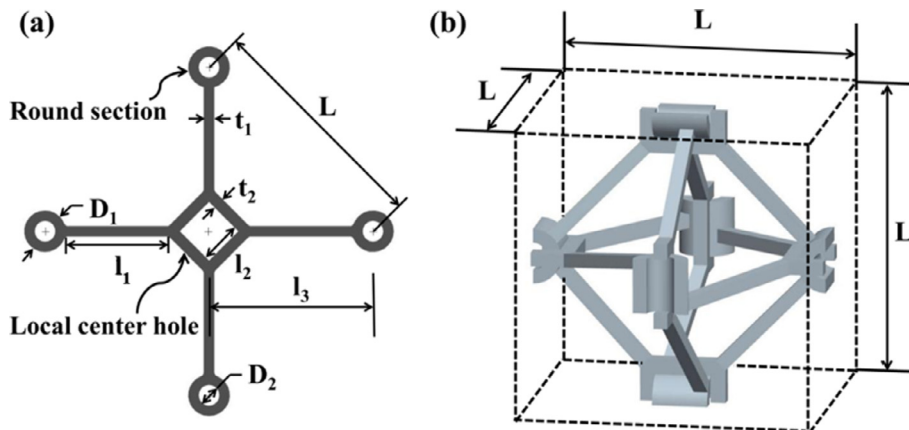


Fig. 1. The geometries of (a) long-fiber reinforced thermoplastic composite part (LFTCP) as building blocks of architected lattice composites, including four round sections (tabs), four struts and a locally central (square) hole; (b) the unit cell of one type of BCC lattice.

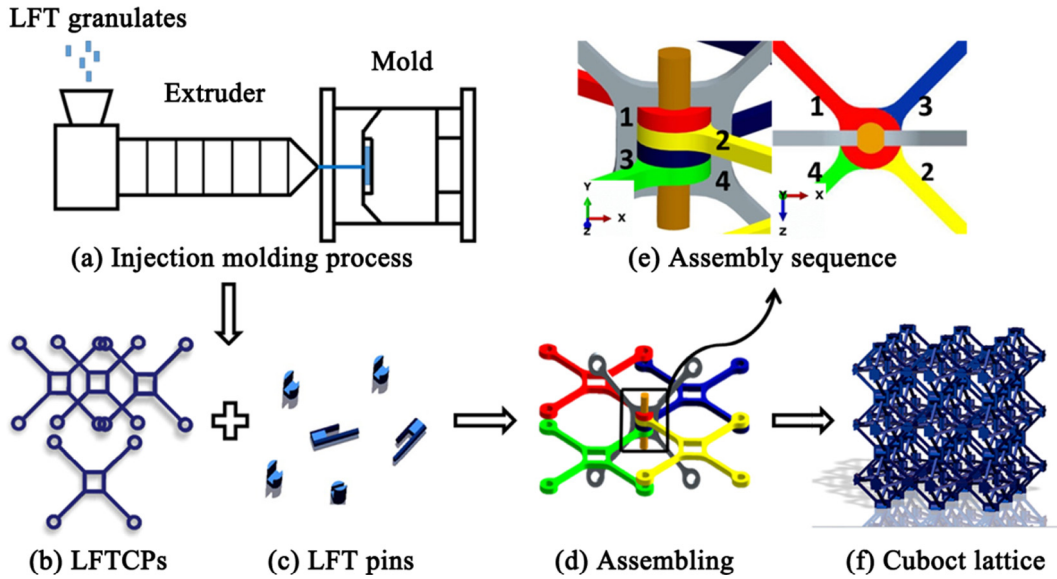


Fig. 2. Schematic illustration for the fabrication procedure of long-fiber reinforced thermoplastic composite lattice structures: (a) Injection molding process for building blocks; (b) the obtained LFTCPs and (c) Long fiber reinforced thermoplastic (LFT) pins; (d) assembly process for an BCC lattice; (e) Detail of the spatial arrangement of tabs in the joints. We define the relative locations of tabs in the square hole is 1-2-3-4 from up to down (Left figure), and the placement of the corresponding struts in the coordinate system here is 1-4-2-3 anticlockwise (Right figure); (f) BCC lattice assembled from planar LFTCPs connected with LFT pins. (For interpretation of the references to color in this figure legend, the reader is referred to the web version of this article.)

and $l_3 = 75$ mm, were selected to give a relative density of the assembled lattice structures of 3%; the latter can be controlled simply by varying the aspect ratio of the struts without changing geometries of connections.

2.3. Parent material tests

Because fibers may break during any stage of the injection molding process, the mechanical properties of the parent materials, which are related to the fiber length and distribution, can be a marked function of the nature of the complex injection process of LFTCPs. To examine this, optical microscopy was first used to measure fiber length of randomly selected samples after incinerating the LFTCPs [25,26], prior to conducting compression tests on struts cut directly from LFTCPs. Specifically, for compression tests, both ends of the struts were adhesively fastened using a nut, as shown in Fig. 4, to prevent stress concentration and instability during compression. Strain gauge extensometers were used to measure the strain during the tests. For repeatability, six randomly selected specimens were prepared for each test.

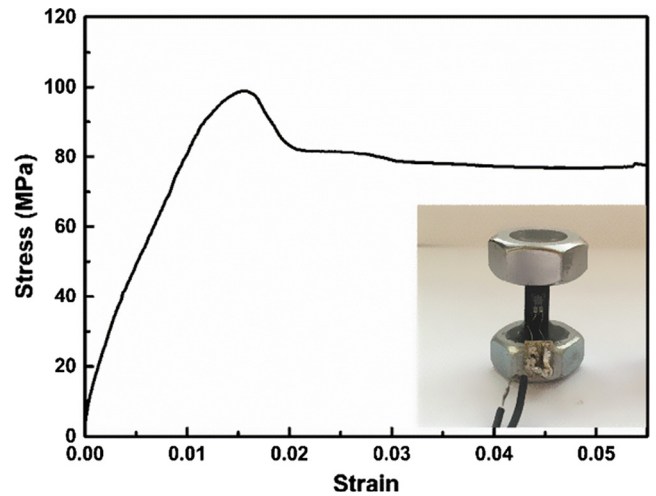


Fig. 4. Compressive stress-strain response of the struts cut directly from LFTCPs. Both ends the struts were adhesively fastened with nuts and compressed.

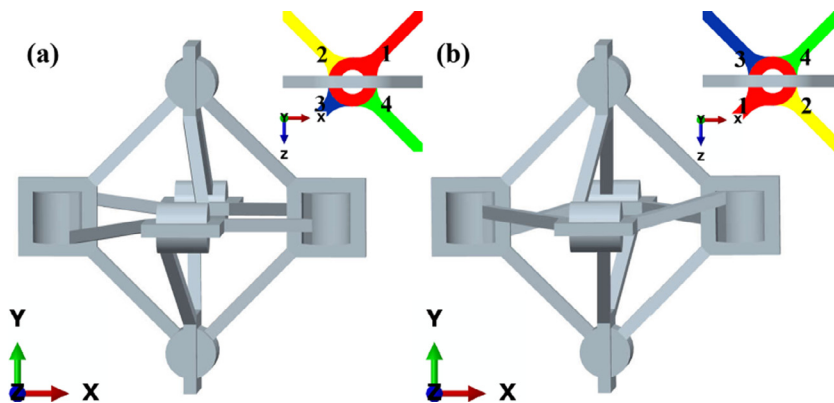


Fig. 3. Long-fiber reinforced thermoplastic composite lattice structures with two different assembly sequences (a) Type I with spatial arrangement of 2-3-4-1; (b) Type II with spatial arrangement of 3-1-2-4. (For interpretation of the references to color in this figure legend, the reader is referred to the web version of this article.)

2.4. BCC lattice tests

As summarized in Table 1, four sets of carbon reinforced thermoplastic BCC lattice unit samples were prepared including two assembly sequences and two fastening connections (injection pins and nylon cable ties), respectively. The regularities of arrangement employed in the present study can be read from the joint to be

Type I assembly sequence of 2-3-4-1 and Type II of 3-1-2-4, as shown in Fig. 3. Set 1 includes Type I unit cells connected by injection pins, Set 2 Type I with nylon cable ties, Set 3 Type II with injection pins, and Set 4 Type II with nylon cable ties.

Out-of-plane compression tests were carried out for the carbon reinforced thermoplastic BCC units at room temperature using an MTS electro servo-hydraulic testing machine (MTS Systems Corp., Eden Prairie, MN, USA) operating at a displacement rate of 0.5 mm/min, in accordance with ASTM standards C365/C364M-05. Displacement measurements were performed during the tests using a laser extensometer with a gauge length of 100 mm. To ascertain that the lattice was firmly placed between the loading platens, the samples were sandwiched between two grooved metal plates which transferred the load to the lattice, as shown in Fig. 5. For repeatability, three specimens were prepared for each set. Additionally, another set of samples (set 5), with the first type of assembly sequence (Fig. 3a) consisting of $2 \times 2 \times 1$ unit cells with nylon cable ties as fastening connection, was also compressed.

Table 1
Grouping details for the six sets of compression tests.

Set	Assembly sequence (shown in Fig. 3)	Connection type	Cell number
1	Type I (2-3-4-1)	Injection pins	1
2	Type I (2-3-4-1)	Nylon cable ties	1
3	Type II (3-1-2-4)	Injection pins	1
4	Type II (3-1-2-4)	Nylon cable ties	1
5	Type I (2-3-4-1)	Nylon cable ties	4
6	Type I (2-3-4-1)	Steel nails	1

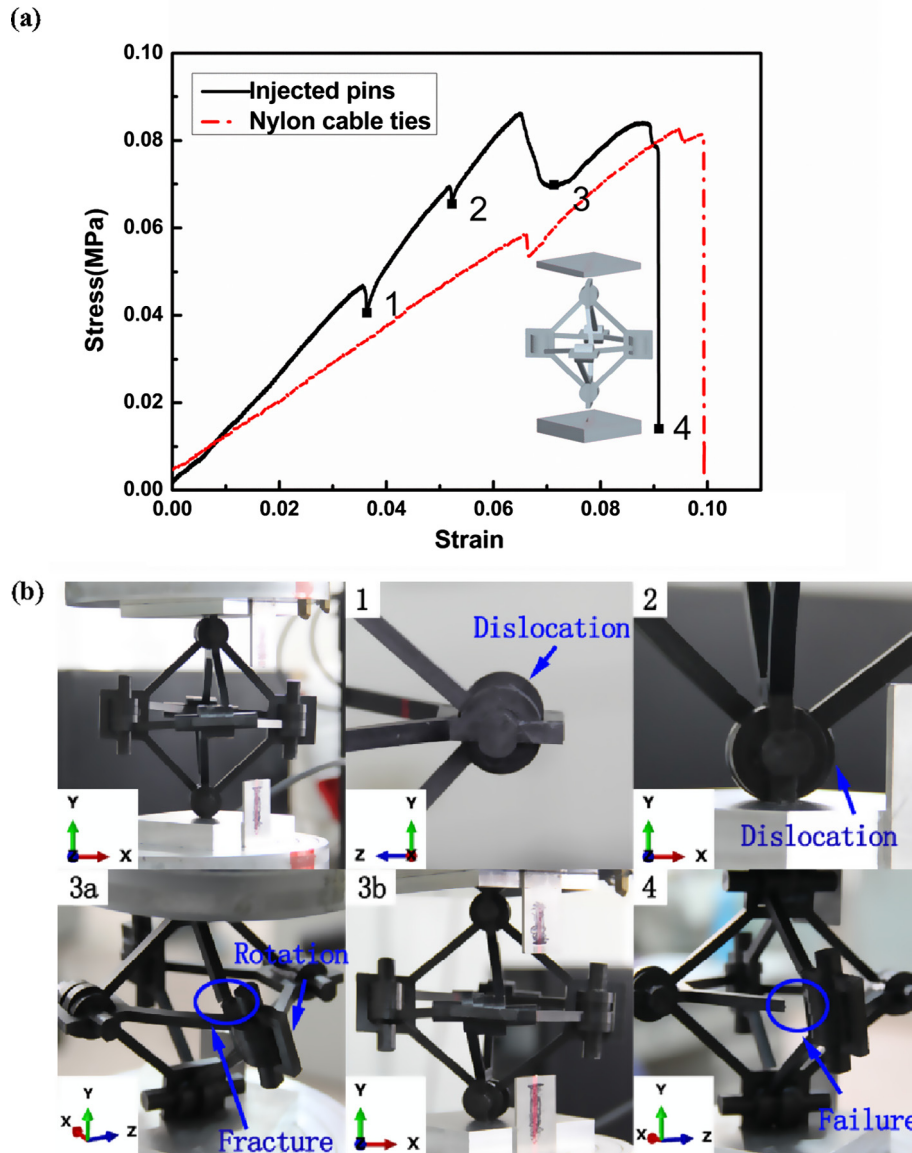


Fig. 5. (a) Compressive stress–strain responses for set 1 (Type I assembly sequence and LFT pins) and set 2 (Type I assembly sequence and nylon cable ties) lattice structures; (b) Photographs showing the deformation characteristics of set 1. (For interpretation of the references to color in this figure legend, the reader is referred to the web version of this article.)

3. Results and discussion

3.1. Parent material characterization

The practical density, ρ_s , of the LFTCPs equals mass divided by volume. Six groups of LFTCPs selected randomly was measured with a scale to get average mass. The volume may be measured directly from the design parameters. The practical density was measured to be 980 kg/m^3 lower than theoretical data. This can be attributed to big number of air voids in the structure which was visible in the SEM pictures. The length of carbon fibers in the LFTCPs, which was measured by optical microscope after incinerating with $565 \text{ }^\circ\text{C}$ in the muffle furnace with nitrogen atmosphere according ASTM D2584-11, was found to be no greater than 2 mm with average length of about 1 mm. The compressive stress-strain response of one injected strut, cut from a LFTCP, is shown in Fig. 4, and indicates a region of elastic response, plastic yielding, a post yield peak stress followed by a plateau region.

The respective compression modulus and strength for the injected strut was measured to be $9.27 \pm 0.1 \text{ GPa}$ and $92.7 \pm 5 \text{ MPa}$.

3.2. Lattice characterization

The nominal compressive stress-strain responses for two types of samples are shown in Figs. 5 and 6. We ascribe the magnitude of the slope of the relatively steady linear curve to the effective modulus. The compression modulus and strength values for the four groups of samples are summarized in Table 2.

Fig. 5a shows the representative compressive stress-strain response for sets 1 (Type I assembly sequence and LFT pins) and 2 (Type I assembly sequence and nylon cable ties) with the corresponding deformation history of set 1, as shown in Fig. 5b. For set 1 with LFT pins, after the elastic deformation regime, two fluctuations occurred concomitant with the sudden dislocation of the four parallel tabs in the central keyhole. Subsequently, the struts buckled, which resulted in an increased deflection of the struts and

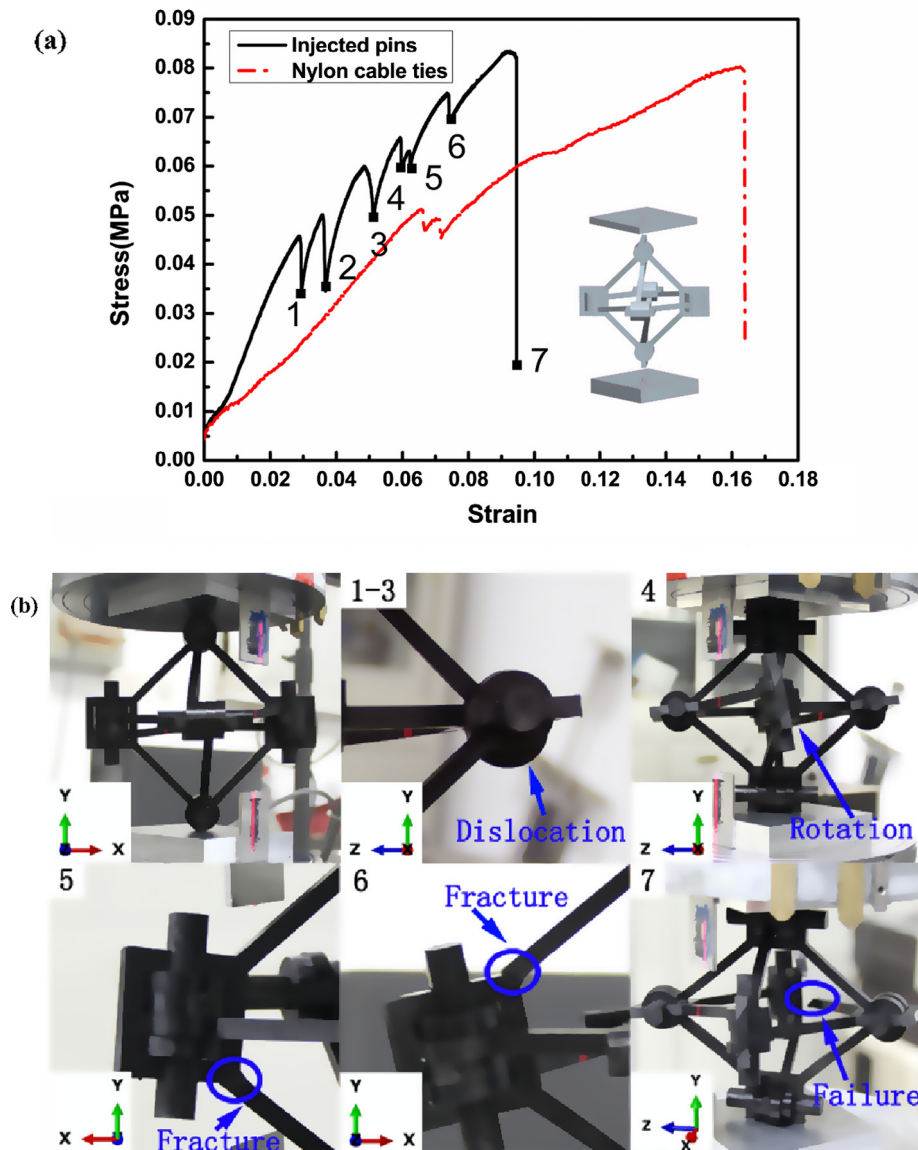


Fig. 6. (a) Compressive stress-strain responses for set 3 (Type II assembly sequence with LFT pins) and set 4 (Type II assembly sequence with nylon cable ties) lattice structures; (b) Photographs showing the deformation characteristics of set 3. (For interpretation of the references to color in this figure legend, the reader is referred to the web version of this article.)

Table 2
Summary of mechanical properties for all the samples. Set 1 is Type I unit cells connected by injection pins, Set 2 Type I with nylon cable ties, Set 3 Type II with injection pins, Set 4 Type II with nylon cable ties, Set 5 Type I $2 \times 2 \times 1$ cells connected by injection pins and Set 6 Type I unit cells with steel nails.

Set	Ultimate force (N)	Compression effective modulus (MPa)	Compression strength (MPa)	Specific stiffness (MPa/(g/cm ³))	Specific strength (MPa/(g/cm ³))
1	967.4	1.41	0.0861	48.96	2.99
2	928.09	0.98323	0.0826	34.14	2.87
3	937.08	1.53528	0.0834	53.31	2.90
4	900.00	0.76773	0.0801	26.66	2.78
5	2837.42	0.85013	0.0693	29.52	2.41
6	1346.07	3.7401	0.1198	129.86	4.16

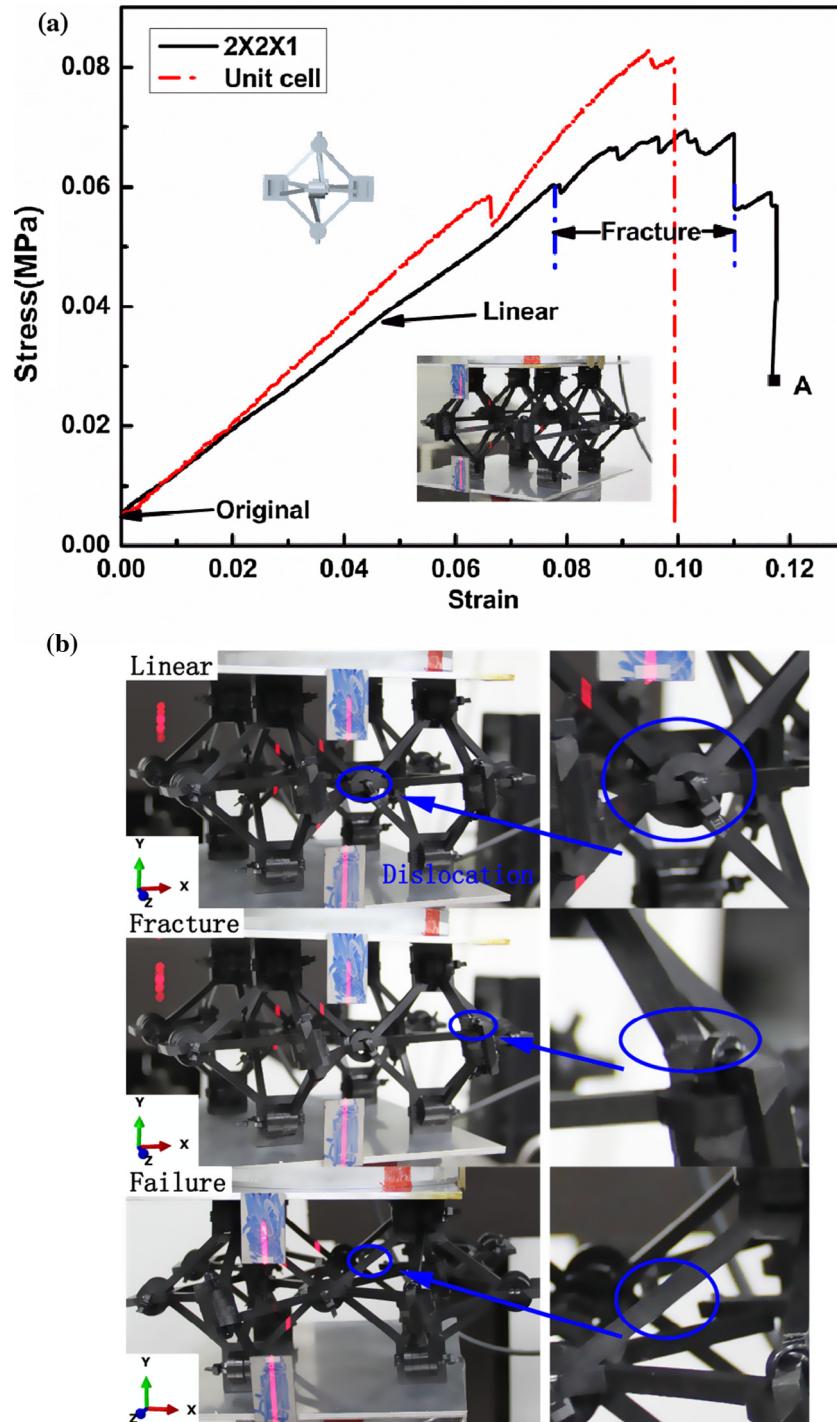


Fig. 7. (a) Compressive stress–strain response for $2 \times 2 \times 1$ samples (Type I assembly sequence and nylon cable ties) comparing with that of set 2 (Type I assembly sequence and nylon cable ties); (b) Photographs showing the deformation characteristics of $2 \times 2 \times 1$ sample. (For interpretation of the references to color in this figure legend, the reader is referred to the web version of this article.)

asymmetrical loading at the nodes that further induced nodal rotation. Meanwhile, the sliding displacement was increased among those four parallel tabs in the central keyhole, which caused fracture of the inclined strut around the central hole corner (shown in Fig. 5b-3a). However, after a degree of self-regulating stability, the compressive stress continued to rise until final failure of the horizontal strut near the round section occurred, as shown in Fig. 5b-4. For set 2 connected by flexible nylon cable ties, a relatively moderate slope was observed at the beginning with less fluctuation than that in set 1. With nylon cable ties as connections, the samples were more flexible and progressive dislocation of the four parallel tabs was observed from the start, before rotary deformation of the whole assembly occurred; this was followed by similar fracture of the inclined strut in the same position around the central hole corner and then final failure of the horizontal strut.

The representative compressive stress-strain response for sets 3 (Type II assembly sequence with LFT pins) and 4 (Type II assembly sequence with nylon cable ties), and the corresponding deformation history of set 3 are shown in Fig. 6. For set 3, following an almost linear regime, several fluctuations occurred before final failure. The first three fluctuations (points 1–3) in the stress-strain curve occurred when dislocation among four parallel tabs took place, while the subsequent three fluctuations (points 4–6) happened with node rotation and the inclined struts fractured at the square hole corner. Indeed, such node rotation caused torsion and bending deformation in the horizontal struts that induced their final fracture, as shown in Fig. 6b-7. For set 4, the stress-strain curve was similar to that of set 2 with different assembly sequence but the same connections. The rotary deformation of the whole structure, along with failure process and mode, was also the same as the samples in set 3 with different connections. With injection pins and nylon cable ties as different joint connections, deformation resistance is again observed to be different, with the structures connected by nylon cable ties being much more flexible. Comparing the compressive response of sets 1 and 3 with different assembly sequences, the fluctuations of set 3 were significantly more marked at the beginning, which demonstrated a weaker capacity of self-regulation to stability of samples compared to set 1. However, with more flexible nylon cable ties as connections, no similar phenomenon was observed. Indeed, by comparing sets 1–3 or sets 2–4, we can attribute the nature of the different rotations for the node and the whole structure to the different assembly sequences.

The through-thickness compressive stress-strain responses for $2 \times 2 \times 1$ samples connected by nylon cable ties are shown in Fig. 7a; they are compared with those of the corresponding unit samples in set 2 with the same assembly sequence and connections. Fig. 7a exhibits characteristics including an elastic deformation region followed with progressive dislocation of the four

parallel tabs observed, and a fluctuated stress region accompanying by fracture of inclined struts around square corner followed by a sudden drop with complete brake of horizontal struts (Fig. 7b). The more obvious fluctuated stress region, in contrast to that in set 2 for unit samples, is attributed to the load bearing capacity of additional lattice trusses. However, the average strength of the whole assembly is lower than that for unit samples in set 2, as discussed in the following section.

3.3. Scanning electron microscopy of fracture surfaces

Fig. 8 shows scanning electron micrographs (SEM) of the fracture surface of struts from all samples. It is apparent that many voids existed in the central region of the struts (Fig. 8a), which is attributed to process defects from the injection molding. The mechanical properties of the LFT composites are influenced by their microstructure (length, orientation and fibers dispersion), which is again affected by the processing conditions (injection velocity) and mold shape. An enlarged image shown in Fig. 8b indicates that fracture of the struts is caused by fiber pullout, fiber fracture, and matrix fracture. Also, it is clear that fiber-matrix interface is relatively weak as the surfaces of many fibers can be seen to be clean with no matrix sticking to them.

3.4. Effects of connections

For a specific assembly sequence, the nature of the joint connection was found to be important for the mechanical properties of the unit cell. From the above tests (Figs. 5 and 6), BCC lattices fastened by injection pins clearly possess higher effective modulus values than those using nylon cable ties. We attribute this to the fact that nylon cable ties are more flexible than injected pins, which results in a gradual and slow dislocation of parallel tabs in the central hole. However, because the injected pins cannot resist the large deformation during compression and thus can break, the compressive strength of samples with these two kinds of connections can only be considered as approximate. Additionally, steel nails were used as another connection option to further examine the effects of connections. Samples with the first type of assembly sequence (Fig. 3a), fastened by steel nails (set 6), were compressed and compared with those fastened by injected pins, as shown in Fig. 9. The effective modulus and strength are significantly increased by 162% and 39%, respectively, without any fluctuation, while the fracture modes of the nail fastened lattices were the same as those for samples connected by injected pins. Note that the steel nails did not fail during the compression process. We can conclude from these observations that connection design, *i.e.*, materials selection and shape design, plays a relevant role in the final properties of the lattice.

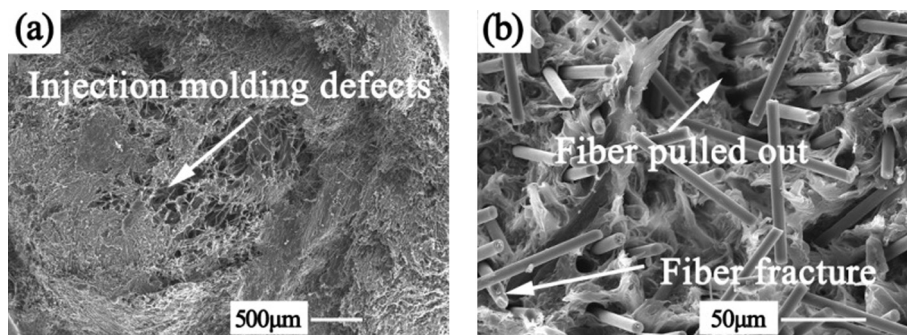


Fig. 8. Scanning electron microscopy images of the fracture surface of the struts. (a) The voids represent injection molding process defects exist in the central of the struts; (b) an enlarged image show fiber pullout and fiber fracture. Also, no matrix sticking on fibers indicates poor fiber-matrix interface inside LFTCPs.

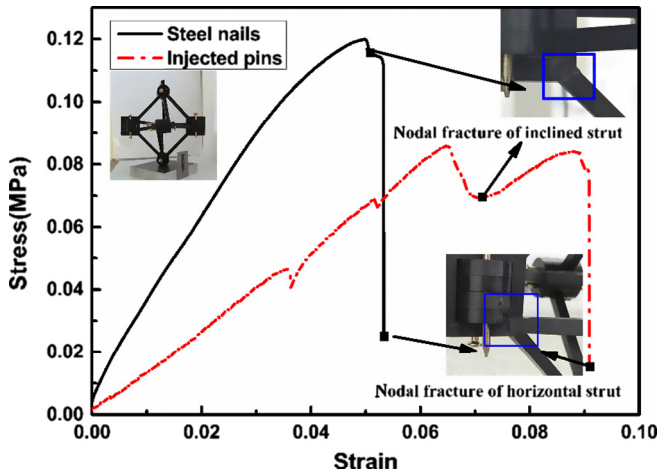


Fig. 9. Compressive stress–strain responses for samples with Type I assembly sequence connected by steel nails, comparing with those of set 2 (Type I assembly sequence and LFT pins). (For interpretation of the references to color in this figure legend, the reader is referred to the web version of this article.)

3.5. Assembly stress analysis

In any actual assembly process, misalignment problems will inevitably exist with the current design for LFTCPs as building blocks. As shown in Fig. 10a, the central point of the round sections in the dark yellow element could not lay in the central plane of the square holes in the red and blue elements. Accordingly, in fabricating the lattice structure, an external force must be applied to

arrange the four tabs at the right location in the square hole during the assembly, which will certainly induce an internal stress into the lattice structure.

It is relevant that such assembly stresses be quantified. To analyze this, a finite element model was developed, using the commercial finite element software Abaqus/CAE, to investigate the stresses caused by the assembly process for the BCC lattice with Type I assembly sequence of 2-3-4-1. The model comprised 30 parts including pins, LFTCPs and round sections; after meshing, it was composed of more than one million elements. The pins were assumed to be rigid and tied to the central hole. In order to ensure the parallel tabs always moved up-and-down along the central line of the pins in the locally central hole with constant relative displacements, twelve connector slots were applied to the tabs and the pins respectively. With no boundary conditions utilized, the migrated displacements were applied to the connector slots according to the actual assembly process of BCC lattice.

Computed values of the equivalent (Von Mises) stress distribution for the structures are shown in Fig. 11, specifically indicating that the maximum stress is located at the strut end near the round section. For all struts with the same displacement, the stress state was found to be the same. Based on a maximum stress criterion and the stress distribution in the struts, it appears that damage may have already existed after assembly in the region where stress is larger than tensile strength of LFTCPs. We conclude, therefore, that the existence of an internal stress induced by the assembly process can degrade the properties of the overall structure. For $2 \times 2 \times 1$ samples in the above tests, the assembly stress is even greater and thus the effective modulus and strength values can be further degraded compared to those for the same type unit cell

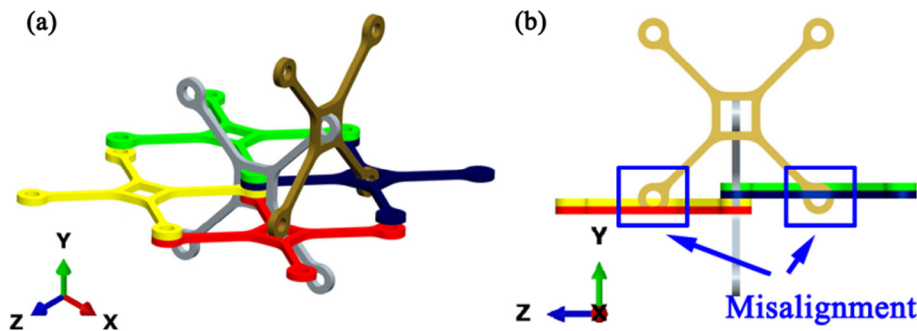


Fig. 10. Misalignments between tabs and central plan of square holes. The central point of the round sections in the dark yellow element should be in the central plane of the square holes in the red and blue elements. (Note that figures a and b are the same assembly from different angles of view). (For interpretation of the references to color in this figure legend, the reader is referred to the web version of this article.)

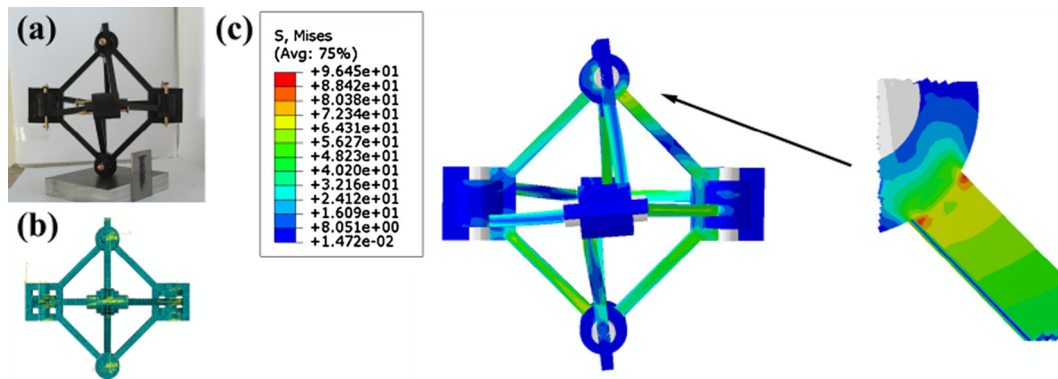


Fig. 11. (a) Sample with Type I assembly sequence connected by steel nails; (b) Meshing of the FEA model with local coordinate systems and reference point; (c) Equivalent (Von Mises) stress distribution of the assembly stress for sample with Type I assembly sequence. The maximum stress is located at the strut ends connected to the round section. (For interpretation of the references to color in this figure legend, the reader is referred to the web version of this article.)

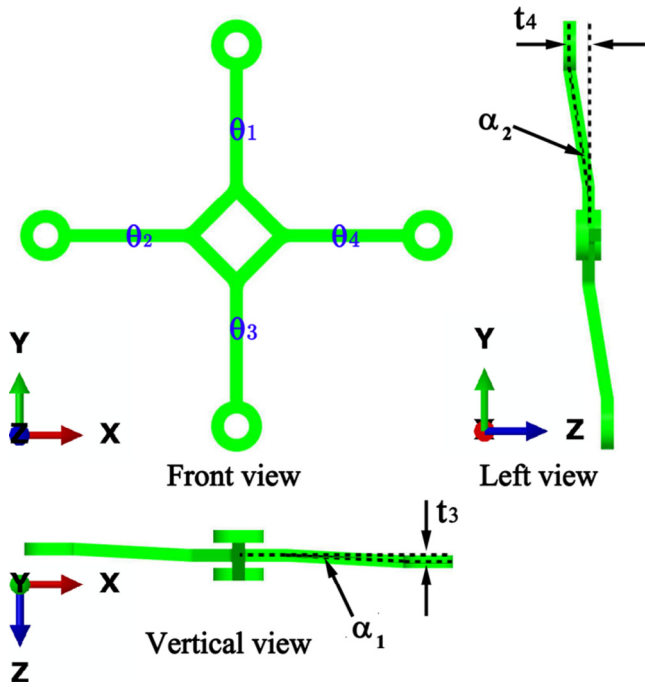


Fig. 12. Three-view drawing for the redesigned digital element of Type III in Table 3. $\theta_1-\theta_4$ are the inclination angles of the four struts to the central plane of the square hole, t_3 and t_4 are the migrated displacements related to the strut thickness with $t_3 = t/2$ and $t_4 = 3t/2$. Two angles α_1 and α_2 can be ascertained according to the geometric relationships, and the values of $\theta_1-\theta_4$ can be related to α_1 or α_2 , as summarized in Table 3 for all the five possible designs of LFTCPs. (For interpretation of the references to color in this figure legend, the reader is referred to the web version of this article.)

Table 3

Five possible types of redesigned LFTCPs. $\theta_1-\theta_4$ are referred to inclination angles of the four struts to the central plane of the square hole, and related to α_1 and α_2 which are ascertained by t and l_1 .

Type	θ_1	θ_2	θ_3	θ_4
I	α_2	α_1	$-\alpha_1$	$-\alpha_2$
II	α_2	α_1	$-\alpha_2$	$-\alpha_1$
III	α_2	$-\alpha_1$	α_1	$-\alpha_2$
IV	α_2	$-\alpha_2$	α_1	$-\alpha_1$
V	α_2	$-\alpha_2$	$-\alpha_1$	α_1

samples. For samples with the same connection, the arrangement of the four tabs in the center hole clearly is critical in affecting the initial assembly stress.

4. Structure redesign

Based on the above assembly stress analysis, the present LFTCPs are clearly not appropriate for large-scale assembly processing and thus mass-production of cellular lattice structures. Therefore, a redesigned LFTCP was developed here. Inclination angles of the four struts to the central plane of the square hole ($\theta_1, \theta_2, \theta_3, \theta_4$), as indicated in Fig.12, were introduced into the novel cross-shaped element. With a given assembly sequence, two angles can be deduced according to the following geometric relationships:

$$\alpha_1 = \sin^{-1}(t_3/l_1), \quad \alpha_2 = \sin^{-1}(t_4/l_1), \quad (2)$$

where geometric parameters α_1 and α_2 are defined, respectively, in Figs. 5a and 12. Parameters t_3 and t_4 are the migrated displacements related to strut thickness with $t_3 = t/2$ and $t_4 = 3t/2$, as shown in Fig. 12. Several different LFTCPs exist, depending upon the different arrangements of the inclination angles. To simplify the complexity of these assemblies, we assume that there is only one assembly sequence in the same structures, which makes $\alpha_1, -\alpha_1, \alpha_2, -\alpha_2$ corresponding to $\theta_1-\theta_4$. For this kind of design, five types of LFTCP units can be created according to the arrangement of the inclination angles of four struts, as summarized in Table 3. There will be further topological designs for BCC lattices, as discussed below. Note that stress concentration should also be taken into account, and chamfers could be a good selection at the strut ends where connected with round section or central hole.

To evaluate the properties of the redesigned structure, an dedicated finite element analysis model was established to simulate the quasi-static compression process of a unit cell assembled by redesigned LFTCPs of Type I (assembly sequence 2-3-4-1). The base of the cell was fully clamped, with the top loaded with a displacement defined by a smooth step amplitude curve to ensure the ratio of kinetic energy to internal energy remained small. The simulated unit cell comprised 30 solid parts including LFTCPs and pins. The pins were assumed to be rigid during the simulation as well. Fig. 13 presents the front and back views of Von Mises stress distribution for the unsymmetrical unit cell. The stress values around the strut ends are larger when connected to the central hole or the round section. Similar to the experimental results for Set 6 with the same assembly sequence and nail connections, the maximum stress appears at the end of the inclined struts, thereby delineating the location of the first failure of an inclined strut. Small rotational deformations were noted to occur at the nodes with offsets. The simulated effective modulus of the unit cell was calculated to be 12.4 MPa, which is 235% higher than that the value 3.7 MPa measured in our experiments for set 6. Based on the computed results, we conclude that the redesigned LFTCPs can induce superior

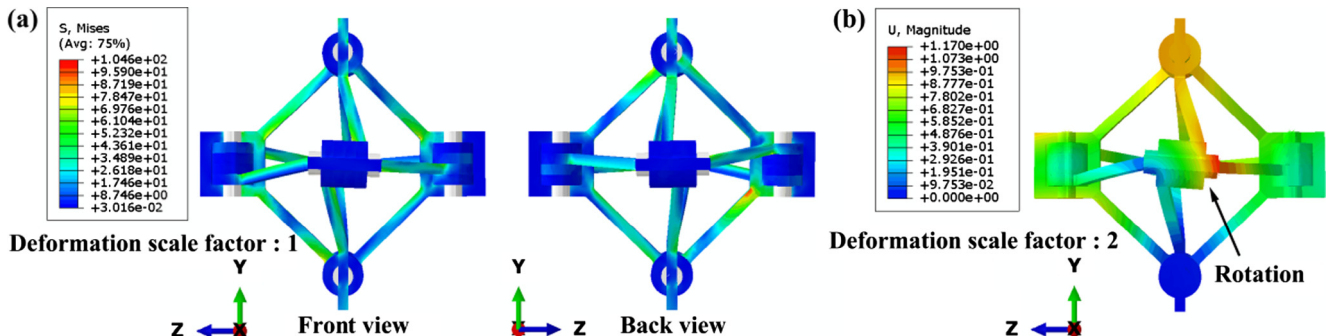


Fig. 13. (a) The front and back view of the Von Mises stress distribution of the Type I tetrahedron lattice structure with an assembly sequence of 2-3-4-1. The maximum stress as shown in back view indicates that failure will first happen at the inclined strut end; (b) Small rotational deformations occurred at the nodes with offset. (For interpretation of the references to color in this figure legend, the reader is referred to the web version of this article.)

mechanical properties in lattice structures, specifically by eliminating damage and possible internal stress created during the initial assembly.

5. Conclusions

In this work, novel, large volume/low cost, thermoplastic composite lattice structures were developed using a reversible assembly (additive manufacturing) methodology involving identical digital elements. Individual digital elements were long-fiber reinforced thermoplastic composite parts (LFTCPs, carbon fiber/PP) obtained by an injection molding approach. Struts in LFTCPs were compressed separately and fiber lengths, after injection, were no greater than 2 mm. Architected lattice structures were fabricated with two specific assembly sequences (defined by spatial arrangement of four struts) and different connections, with the corresponding out-of-plane compressive behavior analyzed and compared. The mechanical performance of the lattice structures was found to be highly sensitive to the joint connections (material property, shape); further, structures with weak connections were observed to be unable to effectively resist deformation and nodal rotation. The effective modulus and strength of the lattice structures fastened by steel nails were significantly higher, by respectively 162% and 39% than those for structures fastened by injection pins. Although the mechanical properties in compression varied only marginally for the different assembly sequences used, the mode of structural deformation, *e.g.*, the rotation direction differed significantly; the failure mode though was unaffected.

To reduce the assembly damage and stress during the assembly process, finite element simulations were used to validate the feasibility of novel design concepts of digital element. A redesigned digital element by introducing four inclination angles of the four struts to the central plane of the square hole, was designed to eliminate the assembly stress and actually enhance the mechanical properties of the newly assembled architectures. One type of redesigned element, with some mature material such as LFT using glass fibre reinforcement, or alternate matrix such as nylon, will be randomly selected to build the lattice structures with stronger connections in the future study. This will also provide a sound direction for further research on superior and low cost lattice structures.

Acknowledgements

This work was supported by the Natural Science Foundation of China (grant nos. 11402012 and 11572021) and Defense Industrial Technology Development Program of China (grant no. A0520131001).

References

- [1] Schaedler TA, Jacobsen AJ, Torrents A, Sorensen AE, Lian J, Greer JR, et al. Ultralight metallic microlattices. *Science* 2011;334:962–5.
- [2] Meza LR, Das S, Greer JR. Strong, lightweight, and recoverable three-dimensional ceramic nanolattices. *Science* 2014;345:1322–6.
- [3] Jang D, Meza LR, Greer F, Greer JR. Fabrication and deformation of three-dimensional hollow ceramic nanostructures. *Nat Mater* 2013;12:893–8.
- [4] Zheng X, Smith W, Jackson J, Moran B, Cui H, Chen D, et al. Multiscale metallic metamaterials. *Nat Mater* 2016. <http://dx.doi.org/10.1038/nmat4694>.
- [5] Valdevit L, Jacobsen AJ, Greer JR, Carter WB. Protocols for the optimal design of multi-functional cellular structures: from hypersonics to micro-architected materials. *J Am Ceram Soc* 2011;94:1–20.
- [6] Evans AG, Hutchinson JW, Fleck NA, Ashby MF, Wadley HNG. The topological design of multifunctional cellular metals. *Prog Mater Sci* 2001;46:309–27.
- [7] Ashby M. Designing architected materials. *Scripta Mater* 2013;68:4–7.
- [8] Fleck NA, Deshpande VS, Ashby MF. Micro-architected materials: past, present and future. *Proc R Soc A* 2010;466:2495–516.
- [9] Zhang JX, Qin QH, Wang TJ. Compressive strengths and dynamic response of corrugated metal sandwich plates with unfilled and foam-filled sinusoidal plate cores. *Acta Mech* 2013;224:759–75.
- [10] Zheng J, Qin QH, Wang TJ. Impact plastic crushing and design of density-graded cellular materials. *Mech Mater* 2016;94:66–78.
- [11] Liu JY, Xiang LL, Man T. The effect of temperature on the bending properties and failure mechanism of composite truss core sandwich structures. *Compos A Appl Sci Manuf* 2015;79:146–54.
- [12] Jiang B, He C, Zhao N, Nash P, Shi C, Wang Z. Ultralight metal foams. *Sci Rep* 2015;5:13825.
- [13] Li WX, Sun FF, Wang P, Fan HL, Fang DN. A novel carbon fiber reinforced lattice truss sandwich cylinder: fabrication and experiments. *Compos A Appl Sci Manuf* 2016;81:313–22.
- [14] Yin S, Wu L, Nutt S. Stretch–bend–hybrid hierarchical composite pyramidal lattice cores. *Compos Struct* 2013;98:153–9.
- [15] Wang B, Wu LZ, Ma L, Sun YG, Du SY. Mechanical behavior of the sandwich structures with carbon fiber-reinforced pyramidal lattice truss core. *Mater Des* 2010;31:2659–63.
- [16] Kazemahvazi S, Khokar N, Hallstrom S, Wadley HNG, Deshpande VS. Confluent 3D-assembly of fibrous structures. *Compos Sci Technol* 2016;127:95–105.
- [17] Malcom AJ, Aronson MT, Wadley HNG. Three-dimensionally woven glass fiber composite struts: characterization and mechanical response in tension and compression. *J Compos Mater* 2016;50:25–43.
- [18] Schneider C, Velea MN, Kazemahvazi S, Zenkert D. Compression properties of novel thermoplastic carbon fibre and poly-ethylene terephthalate fibre composite lattice structures. *Mater Des* 2015;65:1110–20.
- [19] Cheung KC, Gershenfeld N. Reversibly assembled cellular composite materials. *Science* 2013;341:1219–21.
- [20] Margossian A, Bel S, Hinterhoelzl R. Bending characterisation of a molten unidirectional carbon fibre reinforced thermoplastic composite using a dynamic mechanical analysis system. *Compos A Appl Sci Manuf* 2015;77:154–63.
- [21] Schemme M. LFT – Development status and perspectives. *Plast, Addit Compd* 2008;10:38–43.
- [22] Phelps JH, Abd El-Rahman AI, Kunc V, Tucker CL. A model for fiber length attrition in injection-molded long-fiber composites. *Compos A Appl Sci Manuf* 2013;51:11–21.
- [23] Chevali VS, Janowski GM. Flexural creep of long fiber-reinforced thermoplastic composites: effect of processing-dependent fiber variables on creep response. *Compos A Appl Sci Manuf* 2010;41:1253–62.
- [24] Gibson LJ, Ashby MF. Cellular solids: structure and properties. Cambridge (UK): Cambridge University Press; 1999.
- [25] Fliegner S, Luke M, Gumbsch P. 3D microstructure modeling of long fiber reinforced thermoplastics. *Compos Sci Technol* 2014;104:136–45.
- [26] Goel A, Chawla KK, Vaidya UK, Chawla N, Koopman M. Characterization of fatigue behavior of long fiber reinforced thermoplastic (LFT) composites. *Mater Charact* 2009;60:537–44.